THE JOURNAL OF PHYSICAL CHEMISTRY C

Article

pubs.acs.org/JPCC

Si(100) Etching in Aqueous Fluoride Solutions: Parallel Etching Reactions Lead to pH-Dependent Nanohillock Formation or Atomically Flat Surfaces

Brandon S. Aldinger and Melissa A. Hines*

Department of Chemistry and Chemical Biology, Cornell University, Ithaca, New York 14853, United States

ABSTRACT: A dramatic, pH-dependent change in the steady-state chemical and morphological structure of Si(100) surfaces etched in aqueous fluoride solutions is observed with infrared spectroscopy and scanning tunneling microscopy. Low pH solutions ($5 \leq pH \leq 7$), such as the technologically important buffered oxide etchant (buffered HF), produce rough surfaces covered with nanoscale Si{110}-faceted hillocks. In contrast, higher pH solutions ($7.8 \leq pH \leq 10$), including 40% NH_4F (aq.), produce atomically smooth surfaces. The etched surfaces are terminated by a monolayer of H atoms irrespective of pH. The pH-dependent transition is attributed to two competing multistep reaction pathways. At higher pH, the base-catalyzed formation of a surface silanone leads to the production of smooth surfaces. This reaction channel is suppressed at low pH, leading to the formation of {110}-faceted hillocks by a second reaction. The morphological transition is not affected by dissolved O_2 in the etchant.

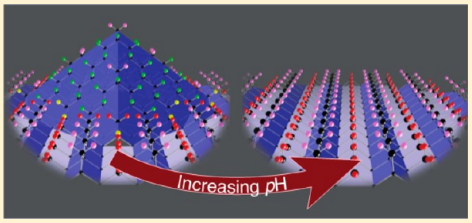

1. INTRODUCTION

As the feature size of micro- and nanoelectronic devices continues to shrink in both production and the research laboratory, the demand for processing chemistries with nanoscale control and precision increases. One particularly important class of reactions are etching chemistries based on aqueous fluoride solutions—mixtures of HF (aq.) and NH_4F (aq.) with pH values ranging from below 1 to ~8. Depending on concentration and pH, these solutions are used in silicon wafer cleaning,[1] to remove certain thin films such as silicon oxide and silicon nitride,[2] and to create silicon surfaces suitable for further chemical functionalization.[3−10] When used with an appropriate pretreatment, these solutions produce extremely clean, near-ideal silicon surfaces that are terminated by a single monolayer of H atoms.

These reactions piqued the interest of the surface science community in the early 1990s when researchers at Bell Laboratories showed that a brief etch in 40% NH_4F (pH 8) followed by a quick H_2O rinse produced ideal atomically flat, H-terminated Si(111) surfaces that are stable in air for tens of minutes.[11] Twenty years later, a similar procedure was developed to produce atomically smooth surfaces on the technologically relevant face of silicon, Si(100).[12] Both reactions use 40% NH_4F at pH ~ 7.8, whereas most industrial processes use acidic fluoride solutions with $pH \leq 5$.

This study seeks a fundamental understanding of these fascinating but complex surface chemistry reactions by asking a seemingly simple question: Is the few-unit pH difference between the solutions used to produce ideal, atomically flat surfaces in the fundamental investigations and those commonly used in industry chemically important? Or does the somewhat lower pH of the industrial solutions simply reduce the etch rate, thereby increasing control? In answering this question, we demonstrate a dramatic and unexpected, pH-dependent change in the steady-state chemical and morphological structure of Si(100) surfaces etched in aqueous fluoride solutions—a change that is explained by the existence of two parallel etching reactions: one dominating at high pH ($pH \geq 7.8$) and another dominating at lower pH ($pH < 7$).

Importantly, we show that solutions favored by industry, including "buffered HF" and "buffered oxide etchant", *intrinsically roughen Si(100) surfaces*, producing surfaces covered entirely by Si{110}-faceted nanoscale hillocks. To circumvent the tip-convolution effects inherent to scanned probe microscopies, a spectroscopic indicator of the hillocked-to-smooth morphological transition is demonstrated.

Etching of silicon in basic or near-basic aqueous fluoride solutions ($pH \geq 4$) is generally thought to occur through a multistep process involving sequential silicon oxidation and silicon removal reactions; however, the specific surface reactions remain unclear. Oxidation reactions involving OH^-, H_2O, and O_2 have been previously proposed,[13−16] whereas the etchant is thought to be HF or an ionic adduct (HF_2^-)[17,18] but not F^-.[19] These solutions produce entirely H-terminated surfaces; however, attempts to spectroscopically characterize the fundamental reactions and the reaction intermediates have been largely fruitless.

2. EXPERIMENTAL SECTION

Silicon wafers were oxidized to a depth of ~100 nm and annealed in sequential exposures to 1 atm O_2 and N_2 at 1100 °C for 30 min each. For STM investigations, Si(100) samples were diced from P-doped, 0.5−10 Ω cm wafers cut to within

Received: August 13, 2012
Published: September 14, 2012

dx.doi.org/10.1021/jp308064s | J. Phys. Chem. C 2012, 116, 21499−21507

0.9° of the (100) orientation. Samples for spectroscopic analysis were cut into 12 mm × 40 mm dice from >1000 Ω cm, double-side-polished, float-zone Si(100) wafers that were either nominally flat or were miscut by 9° toward the [011] direction; the samples were then beveled on their short sides for analysis in the multiple-internal-reflectance geometry. All samples were thoroughly cleaned by sequential baths of warm trichloroethylene, acetone, methanol, and ultrapure water (Millipore Milli-Q).

Immediately prior to each experiment, the oxidized silicon samples were cleaned for 10 min each in sequential basic and acidic peroxide solutions at 80 °C. The basic peroxide solution was composed of 12 M NH_4OH (aq., EMD Chemical, ACS grade), 30% H_2O_2 (J. T. Baker, CMOS grade), and ultrapure water in a 1:1:5 ratio by volume. The acidic peroxide solution was composed of 13 M HCl (aq., J. T. Baker, ACS grade), 30% H_2O_2, and ultrapure water in a 1:1:5 ratio by volume. The samples were thoroughly rinsed in ultrapure water between and after the baths. The thick thermal oxide was then removed by a 75 s etch in buffered oxide etchant (BOE, J. T. Baker, a 5:1 by volume mixture of 50% HF:40% NH_4F). This treatment removed the hydrophilic oxide layer, replacing it with an extremely hydrophobic monolayer of H atoms.[1]

The temporal evolution of surfaces in pH 5 buffered HF was studied by immersing the samples in BOE. In practice, this step was combined with the thermal oxide strip described in the preceding paragraph, leading to reported etch times that were 75 s shorter than the total etch time.

To study the effects of pH on Si(100) etching, a pH-modified solution of 40% NH_4F (pH 7.8) was prepared by gravimetric addition of concentrated HCl or NH_4OH. The sample was then immersed in the etchant for 2 min. During etching, the sample was drawn through the etchant/air interface at ~15 s ($7 < pH < 9$) or ~10 s ($pH \geq 9$) intervals to dislodge H_2 bubbles produced by the etching reaction.[20] This step was crucial to the production of atomically flat surfaces at high pH. Less frequent withdrawal led to degradation of both the vibrational and morphological data. The withdrawal step was omitted for pH < 7 etchants, as few or no bubbles were observed under these conditions. The solution pH was measured after etching with pH-indicator strips (colorpHast, EMD Chemicals) to avoid contamination.

To assess the effects of dissolved O_2, aliquots of NH_4F or BOE were first sparged with Ar (g) for 30–60 min in a sealed enclosure. An oxidized sample was either immersed in BOE for 4 min, or alternatively, the initial oxide layer was removed with a 75 s immersion in untreated BOE, followed by a 30 s etch in sparged NH_4F. To minimize disturbance of the inert atmosphere, the sample was not drawn through the etchant/Ar interface during etching.

After etching, the samples were loaded into an ultrahigh vacuum scanning tunneling microscope (UHV STM) or a dry-air-purged Nicolet 670 Fourier-transform infrared (FTIR) spectrometer equipped with a mercury–cadmium–telluride detector and a ZnSe grid polarizer (Molectron). Spectra of flat surfaces were obtained with both s- and p-polarized radiation. Spectra of vicinal surfaces were obtained with both s- and p-polarized radiation propagating along the [011] and [01$\bar{1}$] directions. The reported spectra were referenced to oxidized samples produced by exposing the etched surfaces for 20 min to species generated *in situ* by a Hg pen lamp. The spectra were computationally transformed from the experimental reference frame to a Cartesian reference frame to obtain the components of the squared transition dipole moment: μ_x^2, μ_y^2, and μ_z^2/ε_z^2, where ε_z is the *z*- (surface normal-) component of the adsorbate dielectric tensor, an unknown constant.[21] On flat surfaces, μ_x^2 and μ_y^2 are identical by symmetry and are reported as $\mu_{\|}^2$. Interference fringes in the spectra were removed computationally.[22]

The etched surfaces were H-terminated and displayed intense absorption bands in the Si–H stretch region (2060–2160 cm^{-1}). Modes associated with subsurface oxidation, silanol formation, or hydrocarbon contamination were notably absent from the spectra.

3. RESULTS

3.1. Estimation of Ionic Species in pH-Modified Solutions. The ionic species present in the pH-modified solutions were estimated by simultaneously solving five equations numerically,[23] using an approach similar to ref 24. The first four equations described the relevant chemical equilibria, namely, the dissociation of HF, HF_2^-, $H_2F_3^-$, and H_2O. The next equation described the conservation of F atoms, which was set to 10.91 M—the nominal concentration of 40% NH_4F. The last equation set the concentration of H^+ to the measured pH. The dissociation constants were taken from refs 24 (fluorine-containing species) and 25 (others).

This approach was first tested by calculating the pH of 40% NH_4F (aq.). This required the inclusion of two additional equations: the dissociation of NH_4OH and the conservation of NH_4-related species. Although neglect of solution nonidealities (e.g., activity coefficients) led to a somewhat lower calculated pH (7.3) than measured (7.8), this approach was judged sufficient for estimation of qualitative trends.

The calculated concentrations of the important ionic species in pH-adjusted NH_4F are shown in Figure 1. As expected, the concentration of OH^- increased with increasing pH, whereas the concentration of the putative etchants (HF, HF_2^-) decreased. The concentrations of HF and HF_2^- had the same functional form, making kinetic distinctions between the two species impossible over this range.

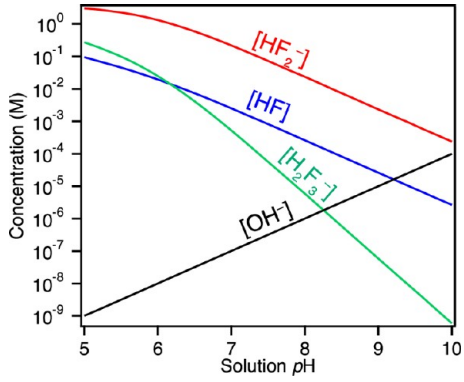

Figure 1. Calculated concentrations of principal species in pH-adjusted NH_4F solutions.

3.2. Evaluating Steady State in Low pH Solutions. We sought to understand the *steady-state chemical structure* of etched surfaces and through this the chemical reactions that created these surfaces. As a surface etches, its structure evolves from an initial state, which is dependent on processing history, to a steady state that is history independent and controlled by the chemical reactions at the surface. During the initial phase of

etching, the nature and concentration of adsorbed species may change due to morphological evolution, such as facet formation or surface smoothing. Once steady state is reached, a statistical sample of surface species or morphologies will show no further evolution even though individual atomic-scale features (e.g., step edges, etch pits) will continue to evolve with time.

A constant etch time for experiments in pH-adjusted NH_4F was chosen from experiments on the assumed slowest etchant, the pH 5 solution. Although the pH-dependent etch rate was not measured directly in these experiments, qualitative trends in etch rate were estimated from the observed rate of H_2 bubble formation, which increased dramatically with increasing pH. This observation was consistent with recent quantitative measurements over a somewhat smaller pH range.[15]

Figure 2 shows that the infrared spectrum of Si(100) etched in the pH 5 solution evolved significantly during the first 2 min

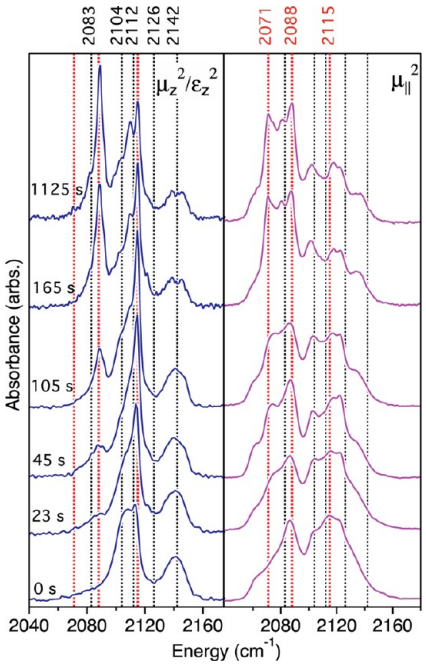

Figure 2. The Cartesian components of the Si−H stretch bands of Si(100) etched in the slowest etchant, pH 5 buffered oxide etchant, evolve with etch time, reaching steady state after approximately 165 s. The principal absorption bands associated with {110} hillocks and atomically smooth (100) faces from Table 1 are indicated by red and black dotted lines, respectively.

of etching, reaching steady state in less than 3 min. After reaching steady state, no further changes were observed even after extended etching. At higher pH, the steady-state structure was reached more quickly. For example, Si(100) surfaces etched in pH 7.8 NH_4F reached steady state in less than 15 s.[12]

On the basis of these data, an etch time of 2 min was used to evaluate the steady-state chemical and morphological structure of etched Si(100) surfaces in solutions with pH ≥ 6, whereas a slightly longer time (2.75 min) was used for pH 5 buffered oxide etchant.

3.3. Chemical Structure Depends on pH. The steady-state chemical structure of Si(100) surfaces etched in pH-modified NH_4F solutions was highly pH dependent, as shown by the infrared spectra in Figure 3. Two different regimes were apparent. In the high pH regime (7.8 ≤ pH ≤ 11), the infrared spectra were pH independent, displaying the five principal

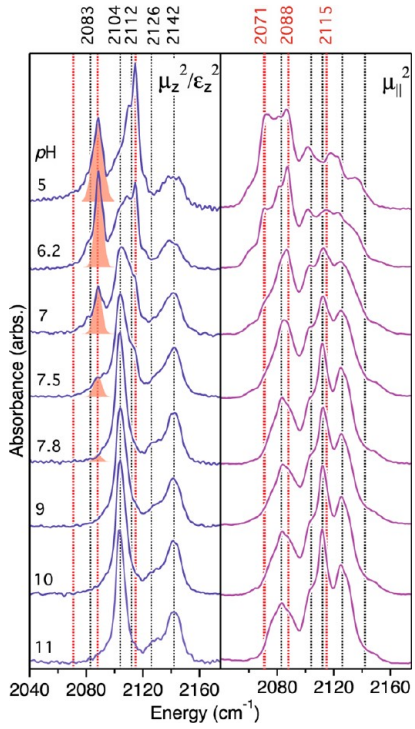

Figure 3. The Cartesian components of the Si−H stretch bands of Si(100) etched to steady state in pH-modified NH_4F show {110}-faceted hillocks increasingly develop as pH decreases below 7.8. Higher pH solutions (pH ≥ 7.8) produce smooth surfaces. The principal absorption bands associated with {110} hillocks and atomically smooth (100) from Table 1 are indicated by red and black dotted lines, respectively. Hillock growth is most easily followed from the growth of the well-resolved, hillock-associated band in z polarization (red-shaded region at 2088 cm^{-1})—the symmetric H−Si{110} stretch.

absorption bands indicated by the black dotted lines and listed in Table 1. As the pH was reduced from 7.5 to 5, three additional bands, indicated by the red dotted lines, increased in intensity, whereas some of the original bands decreased. As discussed below, this spectral evolution showed that high pH solutions produced atomically flat surfaces. Below the critical 7.8 pH, etching produced nanoscale hillocks with predominantly {110} faces. The relative areal density of the nanohillocks increased with decreasing pH over the pH range 7.5−5.

The five absorption bands characteristic of the high pH regime were previously assigned using a combination of polarized infrared spectroscopy, scanning tunneling microscopy, and kinetic Monte Carlo (KMC) simulations.[12,15] These etched surfaces displayed a characteristic striped morphology consisting of alternating, single-atom-wide rows of unstrained dihydrides separated by single-atom-wide trenches terminated by strained, canted dihydrides as illustrated by the STM image and molecular model in Figure 4. The orientation of the rows and trenches is dependent on atomic plane, rotating by 90° on each successive plane. The unstrained dihydrides, which comprised 32% of a monolayer (ML) from KMC simulations,[15] displayed symmetric and antisymmetric Si−H stretch modes at 2104 cm^{-1} (z polarized) and 2112 cm^{-1} (|| polarized), respectively. The strong steric interactions between H atoms on adjacent strained dihydrides (39% ML) are partially relieved by canting as originally suggested by molecular simulations.[26,27]

dx.doi.org/10.1021/jp308064s | J. Phys. Chem. C 2012, 116, 21499−21507

Table 1. The Energy, Polarization, and pH Dependence of the Principal Absorption Bands in the Si−H Stretch Region[a]

energy (cm^{-1})	face	type	Si−H stretch vibration	z-pol	‖-pol	low pH	high pH
2071	{110}	mono	antisymmetric	–	S	•	–
2083	(100)	di	strained, down Si−H	–	S	•	•
2088	{110}	mono	symmetric	S	S	•	–
2104	(100)	di	unstrained, sym.	S	?	–	•
2112	(100)	di	unstrained, antisym.	–	S	–	•
2115	{110}	mono	strained	S	?	•	–
2126	{111}	mono	strained	w	S	–	•
2142	(100)	di	strained, up Si−H	S	–	•	•

[a]Intensity: S = strong, w = weak, – = not observed, and ? = unknown due to spectral congestion.

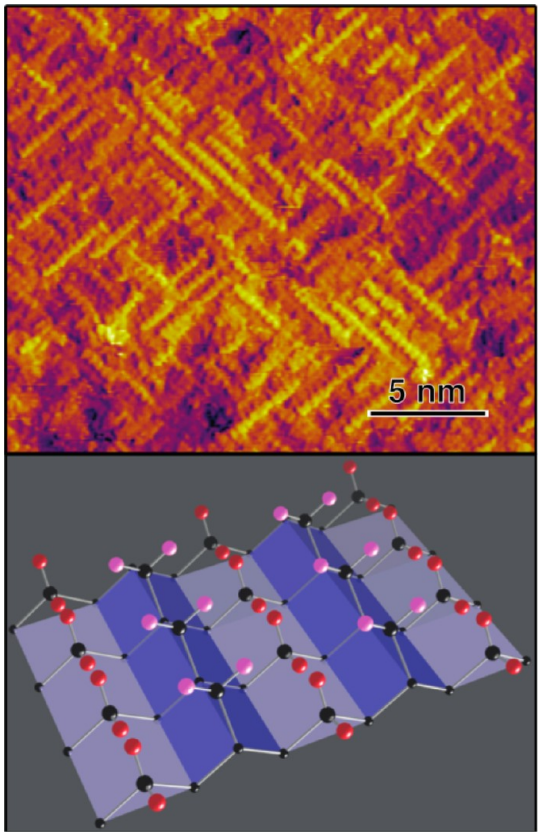

Figure 4. The structure of Si(100) surfaces etched to steady state in unadulterated 40% NH_4F (pH 7.8). (top) STM image and (bottom) molecular model of surface showing alternating rows of unstrained dihydrides and trenches of strained dihydrides. Si atoms are black, and strained and unstrained H atoms on silicon dihydrides are red and pink, respectively.

This canting decouples the motion of the two Si−H bonds, leading to isolated stretch vibrations of the "down" and "up" Si−H bonds at 2083 cm^{-1} (‖ polarized) and 2142 cm^{-1} (z polarized), respectively. The mode at 2126 cm^{-1} (primarily ‖ polarized) is assigned to the Si−H stretch mode of a particular type of strained monohydride (20% ML) that occurs primarily at the intersection of a stripe and a perpendicular trench, as shown in Figure 5. These monohydrides have three backbonds to bulk Si atoms and are thus termed "{111}-type strained monohydrides", as shown in Table 1.

Below the critical pH of 7.8, three additional absorption bands increased in intensity. The energies and polarizations of two of these bands allowed their incontrovertible assignment to the antisymmetric (2071 cm^{-1}, ‖ polarized) and symmetric

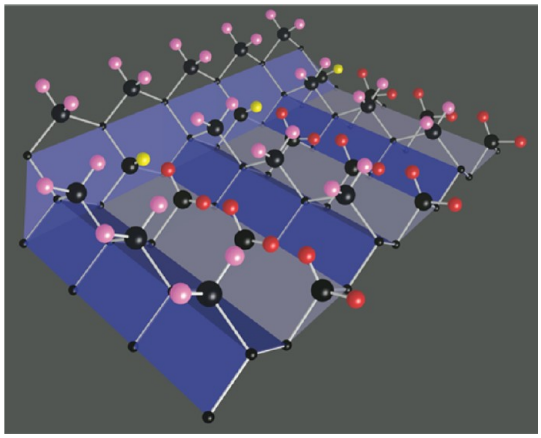

Figure 5. Strained {111}-type monohydrides, shown in yellow, occur at the intersection of an unstrained dihydride row and a perpendicular strained dihydride trench. According to kinetic Monte Carlo simulations,[15] the density of these sites on NH_4F-etched Si(100) is 20% ML, consistent with the relatively intense absorption band at 2126 cm^{-1}.

(2088 cm^{-1}, both polarizations) vibrations of monohydrides bound to Si{110} microfacets. The energies of these bands were in good agreement with the antisymmetric and symmetric stretch modes of monohydrides on flat NH_4F-etched Si(110), which are observed at 2070.8 and 2089.4 cm^{-1}, respectively.[28,29] On Si(110) surfaces, the antisymmetric and symmetric stretch vibrations are aligned with the [001] and [110] directions, respectively. By symmetry, Si{110} microfaceting of a Si(100) surface will lead to equal densities of $(1\bar{1}0)$-, (101)-, (110)-, and $(10\bar{1})$-oriented microfacets, each oriented 45° from the (100) surface normal. The symmetric monohydride stretch vibrations of the {110} microfacets will be aligned with the microscopic facet normals, which is consistent with the significant absorption intensity of the 2088 cm^{-1} band in both polarizations. In contrast, the antisymmetric monohydride stretch vibration of the {110} microfacets will be aligned with the $\langle 00\bar{1}\rangle$, $\langle 0\bar{1}0\rangle$, ⟨001⟩, and ⟨010⟩ directions. These directions are all perpendicular to (100), consistent with the intense 2071 cm^{-1} absorption band being observed only in ‖ polarization (i.e., negligible intensity in z polarization).

Importantly, the spectra in Figure 3 rule out significant Si{111} microfacet formation at any pH. NH_4F-etched Si(111) surfaces display a single intense, [111]-oriented absorption band at 2083.6 cm^{-1}.[30] If Si{111} microfacets were present, a strong absorption band at this energy would be observed in both polarizations, as the {111} microfacets would each be oriented 54.7° from the (100) surface normal. This band is notably absent from the z-polarized spectra in Figure 3. In

dx.doi.org/10.1021/jp308064s | J. Phys. Chem. C 2012, 116, 21499−21507

contrast and for comparison, this band is readily observed at 2081.3 cm^{-1} on H_2O-etched Si(100) surfaces in both polarizations,[31] where the ~2 cm^{-1} red shift on H_2O-etched surfaces is attributed to reduced dipole−dipole coupling on the microfacets.[32,33]

We assigned the final absorption band, which appeared at 2115 cm^{-1} in the *z*-polarized spectrum, to the vibration of "{110}-type strained monohydrides", which by geometry must encircle the base of the {110} microfacets. In contrast to {111}-type strained monohydrides, these species, seen in yellow in Figure 6, are backbonded to other hydrides, which presumably

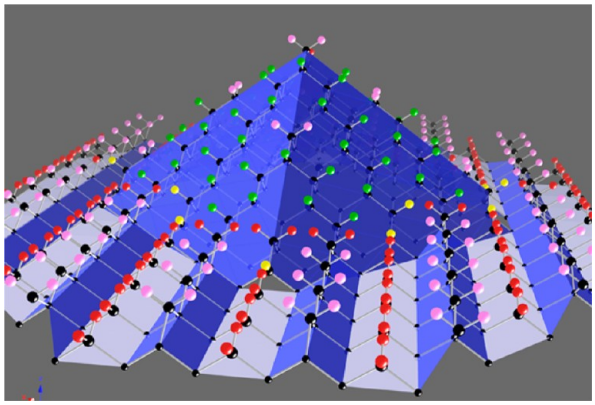

Figure 6. Molecular model of an ideal, {110}-faceted hillock on a flat Si(100) surface rising from an ideal alternating row geometry. Unstrained H atoms on silicon monohydrides are green, whereas the corresponding strained H atoms are yellow. Vibrational excitation of the green atoms in this image would lead to absorption at 2071 and 2088 cm^{-1}. In contrast, vibrational excitation of the yellow atoms, which are strained {110}-type monohydrides, would lead to absorption at 2115 cm^{-1}.

leads to their distinct vibrational energy. This assignment is supported by similar magnitudes of the 11 cm^{-1} shift in vibrational energy between the {111}- and {110}-type strained monohydrides and the 7.9 cm^{-1} shift between H−Si(111) and the center of the H−Si(110) bands on flat surfaces. Unfortunately, the polarization of this band could not be precisely measured, as this region of the ||-polarized spectrum is congested. However, this band is readily observed on H_2O-etched Si(100) surfaces in both polarizations, which is consistent with the orientation of the {110}-type strained monohydrides.

In making this assignment, we note that the identity of the 2115 cm^{-1} band has been the subject of significant speculation and controversy, with most attributing this feature to some type of dihydride stretch mode (a strained canted dihydride,[31] horizontal dihydrides on {111} microfacets,[34] an asymmetric dihydride,[35] or other[36]). The assignment to the strained canted dihydride can be definitively ruled out from studies of NH_4F/Si(100) etching which assign vibrational bands at 2083 and 2142 cm^{-1} to this species.[12,15] Furthermore, the absence of a second unassigned band that is correlated in intensity with the 2115 cm^{-1} mode suggests this band is not associated with a dihydride or trihydride species. Finally, the absence of {111} microfacets suggests this feature is not associated with {111}-type strained monohydrides.

In summary, the three additional absorption bands that appear with increasing intensity below the critical pH of 7.8 are assigned to the production of strained and unstrained silicon monohydrides on {110} microfacets. Importantly, vibrational spectroscopy cannot distinguish faceted hillocks from faceted etch pits, nor can it distinguish between perfect (pyramidal) and rounded (vicinal) microfacets.

3.4. Morphology Depends on pH: Nanohillock Formation below pH 7.8. The steady-state morphology of Si(100) surfaces etched in pH-modified NH_4F solutions was highly pH dependent, as shown by the STM images in Figure 7. Again, two distinct regimes were observed. In the high pH regime ($7.8 \leq pH \leq 11$), the morphologies were pH independent, displaying the characteristic alternating row morphology observed with etching in unadulterated 40% NH_4F (aq.) solutions. As the pH dropped from 7.8 to 7.0, the surface developed an increasing density of nanoscale hillocks (protrusions) with heights in the range of 0.5 nm. The shape of these protrusions could not be reproducibly imaged because of tip convolution effects. Below a pH of 7.0, the steady-state morphology was very rough. Because of tip convolution, STM images in this pH regime almost certainly *underestimate* the actual surface roughness.

The STM images are consistent with the spectroscopic assignments of the previous section, and confirm the dramatic morphological transition between low pH and high pH.

3.5. Surface Miscut Has Little Effect at Low pH. When miscut Si(100) surfaces are etched in 40% NH_4F (aq.), preferential etching of the row ends leads to the preferential production of long and short single-atom-wide rows parallel and perpendicular to the nominal step direction.[15] This spontaneous symmetry breaking enabled the quantitative understanding of NH_4F etching chemistry.

To check for similar effects in the low pH regime, the Cartesian components of the polarized infrared absorption spectrum of surfaces miscut by 9° toward the [011] direction and etched in pH 5 buffered HF were measured, as shown in Figure 8. The two in-plane components of the spectrum are virtually identical, showing that no such symmetry breaking occurs in low pH solutions. As suggested by the STM images in the previous section, this finding suggests that row-end etching is not the dominant site-removal mechanism in low pH solutions.

3.6. Dissolved O_2 Has Little Effect. The smoothest H/Si(111) surfaces are produced in deoxygenated NH_4F solutions,[37] as the presence of dissolved O_2 in the etchant leads to the nucleation of tiny etch pits.[38] To test for similar effects in Si(100) etching, the infrared spectra of Si(100) surfaces etched in as-received and deoxygenated buffered HF were compared at both pH 5 and pH 7.8. No significant differences were observed (not shown). This finding suggests that the rate of Si(100) oxidation by dissolved O_2 is too slow to compete significantly with etching, at least in the pH range studied.

4. DISCUSSION

These data prove incontrovertibly that the mildly acidic aqueous fluoride solutions commonly used in microelectronics processing, often known as "buffered HF (BHF)" or "buffered oxide etchant (BOE)," *intrinsically roughen Si(100) surfaces on the atomic scale*. This roughening is not due to dissolved O_2 in the etchant. In contrast, similar solutions with a modestly increased pH, including 40% NH_4F, produce atomically smooth surfaces. At the total fluoride concentrations studied here (10.9 M), the transition from rough to smooth surfaces occurs over a

dx.doi.org/10.1021/jp308064s | J. Phys. Chem. C 2012, 116, 21499−21507

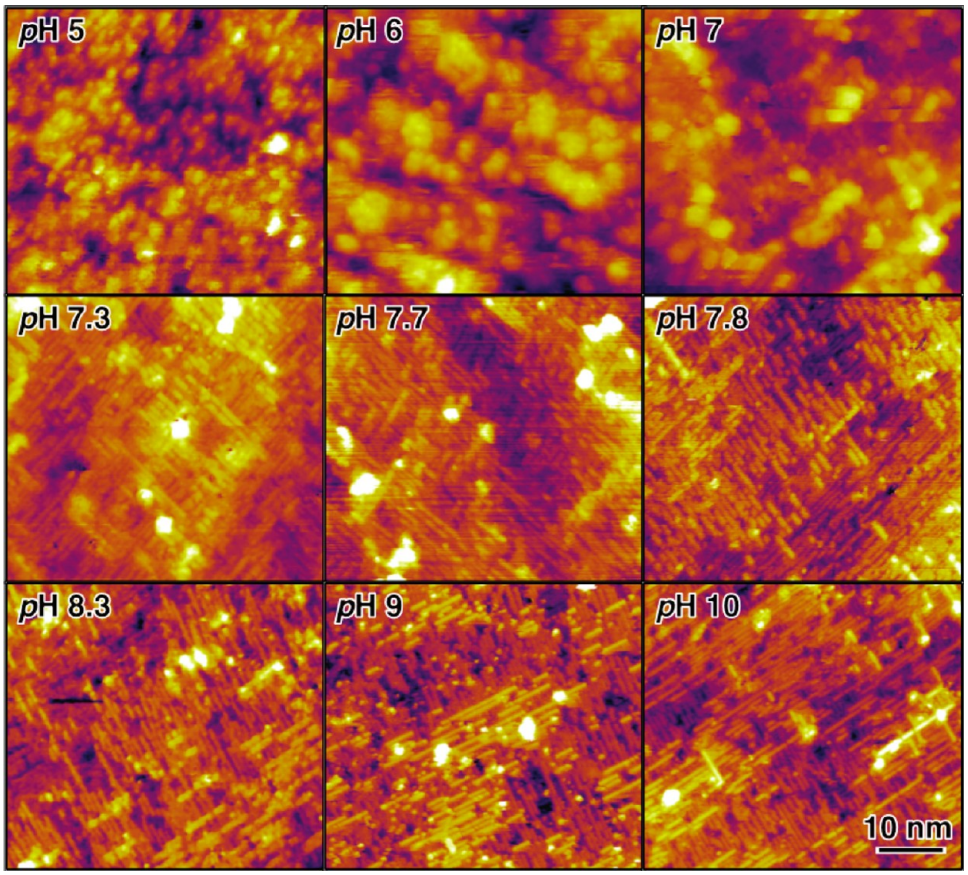

Figure 7. STM images of the steady-state morphology of Si(100) surfaces etched in pH-modified NH_4F solutions show hillock formation at pH ≤ 7 and atomically flat surfaces at pH ≥ 7.8. The pH is indicated in the upper left-hand corner of each image.

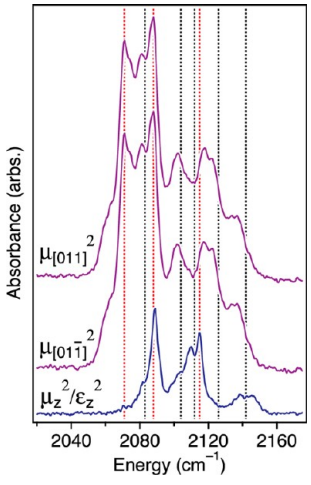

Figure 8. Cartesian components of the polarized infrared absorbance spectrum of Si(100) miscut by 9° toward the [011] direction and etched for 20 min in pH 5 buffered oxide etchant The two in-plane components (purple) are nearly identical, indicating that the etch morphology was not affected by the miscut at this pH. The principal absorption bands associated with {110} hillocks and atomically smooth (100) from Table 1 are indicated by red and black dotted lines, respectively.

narrow pH range and is complete at pH 7.8, as shown in Figures 3 and 7.

Even though all solutions studied in the pH range 7.8−10 formed chemically and morphologically identical, atomically flat Si(100) surfaces, the lowest pH solution (40% NH_4F at pH 7.8) was preferable from a processing perspective. These reactions evolve H_2 gas, which forms transient bubbles on the etching surface.[20] These bubbles must be periodically removed from the surface during etching to prevent mesoscale roughening. Bubble removal becomes increasingly difficult as the pH increases, as the rate of H_2 gas evolution and the overall etch rate increase dramatically with increasing pH.

4.1. Etch Mechanism and Evidence for Parallel Etching Reactions. The dramatic, pH-dependent change in steady-state chemical structure and etch morphology suggests there are two parallel etching (i.e., silicon removal) reactions: one dominating at high pH (pH ≥ 7.8) and another dominating at lower pH (pH < 7).

The high pH data are consistent with the proposed mechanism of Si(100) etching in NH_4F solutions, which is outlined in reactions 1−4 of Figure 9.[15] In this mechanism, the H-terminated silicon surface is slowly attacked by either OH^- or H_2O to form a surface silanol (≡Si—OH) (reaction 1), which can reversibly deprotonate in basic media (reaction 2) to form a siloxy anion. Neither of these reactions are sterically constrained, and they are both expected to be relatively site unspecific (isotropic). If the deprotonated silanol is bonded to an adjacent silicon hydride, such as a row-end site, the siloxy anion can convert to a silanone with simultaneous cleavage of one Si−Si backbond (reaction 3). As explained in ref 15, this reaction places severe steric requirements on the reacting site, as the reacting Si center must undergo a large distortion while a H atom is inserted across the dissociating backbond. These steric requirements explain the formation of the characteristic

dx.doi.org/10.1021/jp308064s | J. Phys. Chem. C 2012, 116, 21499−21507

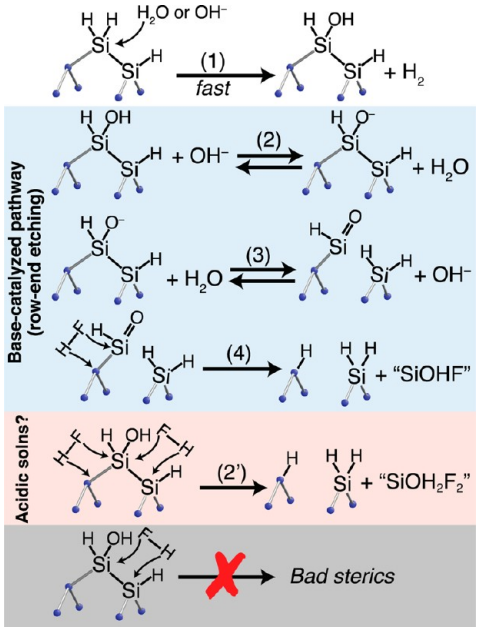

Figure 9. Possible mechanisms for the etching of Si(100) in pH-modified aqueous fluoride solutions. The base-catalyzed mechanism (reactions 1−4, blue background) explains the production of atomically flat surfaces in high pH solutions and is backed up by kinetic Monte Carlo simulations and etch rate data.[15] A concerted mechanism (reactions 1 and 2′, pink background) may be important in acidic solutions, explaining the transition to {110}-hillocked morphologies. Sequential cleavage of silanol backbonds (reactions 1 and X, gray background) is sterically disfavored.

alternating row morphology. Once formed, the remaining Si−Si backbond on the silanone is subject to attack by HF, leading to the production of a solvated silicon species (SiOHF, which will be rapidly hydrolyzed in aqueous solutions) and a H-terminated surface.

As shown in Figure 10, this reaction mechanism is consistent with the measured kinetics, displaying an etch rate

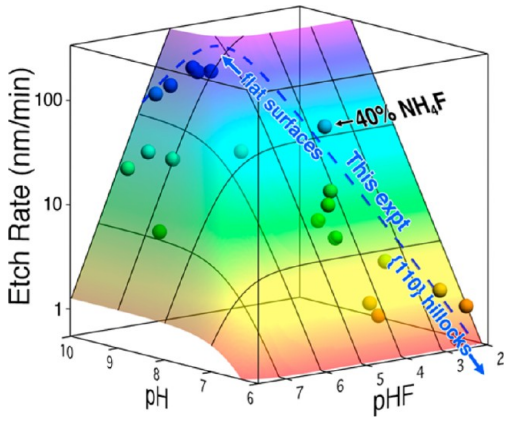

Figure 10. The concentration dependence of the base-catalyzed reaction mechanism (surface) is in good agreement with the measured etch rates (spheres).[15] The pH-modified NH_4F solutions studied here fall along the blue dashed line, which represents the intersection of the calculated solution concentrations with the best-fit kinetics. The regimes that produce atomically flat surfaces (high pH) and {110}-hillocked surfaces (low pH) are labeled.

$$R = \frac{c_1[OH^-][HF]}{c_2[OH^-] + [HF]'} \quad (1)$$

where c_1 and c_2 are constants. The blue dashed line in Figure 10 represents the approximate concentrations of the solutions studied here. This mechanism has two limiting regimes: OH^- limited at low pH and HF limited at high pH. In Figure 10, the two regimes can be visualized as two intersecting planes. Interestingly, atomically flat surfaces are formed close to and on either side of this (broad) intersection. In other words, atomically flat surfaces are formed when the oxidation and etching reactions have comparable rates; both reactions are important and neither can be considered rate limiting. Surfaces with {110} hillocks are produced in a much slower etching regime—a regime where reaction 2 is essentially quenched for lack of OH^-.

Although the pH at which the transition from HF-limited to OH^--limited reactivity occurs is affected by the pK_a of the surface silanol (i.e., the equilibrium constant of reaction 2), the transition pH is not (necessarily) equal to the pK_a. Silanols are somewhat more acidic than the corresponding alcohols; however, the behavior of model organosilanols suggests the surface silanol has a pK_a of ~14,[39] which is far above the morphological transition point. (We note that silanols on *silica* surfaces are much more acidic, having pK_a's of 5−10.[40,41])

By itself, this mechanism does not provide a ready explanation for the pH-dependent steady-state morphology. If reactions 1−4 were the only allowed reactions, the reaction rate would drop exponentially with decreasing pH in the low pH regime, but the site-specificity of the reactions, and thus the steady-state morphology, would likely be unaffected. This is not observed.

A more likely possibility is that a second etching channel becomes dominant in the low pH regime. The formation of {110}-faceted hillocks (as opposed to randomly rough surfaces) suggests that this etching channel is also site-specific (i.e., anisotropic). Without further spectroscopic or simulation data, we can only speculate on the nature of this channel. One possibility, sketched in Figure 9, is that the high concentrations of [HF] and [HF_2^-], the putative etchants, enable concerted reactions such as reaction 2′ that would otherwise be entropically disfavored. For example, first-principles calculations[18] on model compounds suggest that formation of a surface silanol (reaction 1) lowers the activation barrier to backbond cleavage by HF. The problem is that most surface sites on Si(100) have two backbonds to the surface, and sequential cleavage reactions would produce an unrealistically strained reaction intermediate (reaction X).[42] A concerted reaction mechanism would avoid the production of the highly strained intermediate. Other reactions are possible as well, including an acid-catalyzed oxidation reaction[43,44] or a photo- or electrochemical reaction.[9,14,45]

4.2. Key Spectral Indicators of Si(100) Faceting and Hillock Formation. A chemical and morphological understanding of the structure of Si(100) surfaces etched in aqueous solutions has been hindered by the complexity of the Si−H stretch vibrational spectrum. Most researchers (including us) have used the very sensitive multiple-internal-reflection (MIR) geometry; however, the raw spectra obtained in this geometry have many overlapping bands even when polarization analysis is performed. Unambiguous spectral signatures of hillock formation are only evident after the spectra are deconvoluted

dx.doi.org/10.1021/jp308064s | J. Phys. Chem. C 2012, 116, 21499−21507

into their Cartesian components. To aid future researchers, we provide the following guidance.

The key spectral indicators of {110} facet formation on Si(100) surfaces are the intense absorption band at 2071 cm^{-1}, which is only observed in || polarization, and the intense absorption band at 2088 cm^{-1}, which is observed in *both* polarizations. The key spectral indicator of {111} facet formation, which was observed for H_2O-etched surfaces[31] but not in this study, is an intense absorption band at 2081 cm^{-1} which is observed in both polarizations. Importantly, atomically flat Si(100) surfaces display an intense mode at 2083 cm^{-1} in || polarization, which can easily be confused for a {111} or {110} mode unless the polarization dependence is carefully checked. We consider polarization analysis a much more reliable indicator of mode identity than band energy, as dipole coupling is understood to cause significant, morphology dependent shifts (~5 cm^{-1}) in Si−H stretch modes[32,33,46] in addition to shifts caused by interadsorbate steric strain.

4.3. Hillock Morphology. The perfection of the {110}-faceted hillocks produced in low pH solutions remains an open question. Although a perfect square pyramid is sketched in Figure 6 for both aesthetic and pedagogical reasons, the experimental data are equally consistent with more rounded hillocks terminated by vicinal Si{110} microfacets. Interestingly, the spectroscopic data show that there is little, if any, {111} facet formation.

5. CONCLUSIONS

A dramatic, pH-dependent change in the steady-state chemical and morphological structure of Si(100) surfaces etched in aqueous fluoride solutions has been observed. The low pH etchants favored by industry, including buffered HF or buffered oxide etchant with $5 \leq pH \leq 7$, produce surfaces covered with nanoscale Si{110}-faceted hillocks. In contrast, higher pH solutions ($7.8 \leq pH \leq 10$), including 40% NH_4F, produce atomically smooth surfaces. This transition is attributed to two competing reaction pathways. At higher pH, the base-catalyzed formation of a surface silanone leads to smooth surface formation. This reaction channel is suppressed at low pH, leading to the formation of {110}-faceted hillocks by a second reaction.

AUTHOR INFORMATION

Corresponding Author

*E-mail: Melissa.Hines@cornell.edu. Phone: +1-607-255-3040.

Notes

The authors declare no competing financial interest.

ACKNOWLEDGMENTS

This work was supported by the National Science Foundation (NSF) under Award No. CHE-0911405 and made use of the Cornell Center for Materials Research Shared Experimental Facilities which are supported through the NSF MRSEC Program (Grant DMR-1120296). B.S.A. gratefully acknowledges support from the NSF IGERT program (NSF Award DGE-0654193).

REFERENCES

(1) Chabal, Y. J.; Higashi, G. S.; Small, R. J. *Handb. Semicond. Wafer Clean. Technol.* **2008**, 523−618.
(2) Elwenspoek, M.; Jansen, H. V. *Silicon Micromachining*; Cambridge University Press: Cambridge, U.K., 2004; p 420.
(3) Linford, M. R.; Fenter, P.; Eisenberger, P. M.; Chidsey, C. E. D. *J. Am. Chem. Soc.* **1995**, *117*, 3145−3155.
(4) Bansal, A.; Li, X.; Lauermann, I.; Lewis, N. S.; Yi, S. I.; Weinberg, W. H. *J. Am. Chem. Soc.* **1996**, *118*, 7225−7226.
(5) Boukherroub, R.; Morin, S.; Sharpe, P.; Wayner, D. D. M.; Allongue, P. *Langmuir* **2000**, *16*, 7429−7434.
(6) Buriak, J. M. *Chem. Rev.* **2002**, *102*, 1271−1308.
(7) Eves, B. J.; Sun, Q.-Y.; Lopinski, G. P.; Zuilhof, H. *J. Am. Chem. Soc.* **2004**, *126*, 14318−14319.
(8) Michalak, D. J.; Amy, S. R.; Aureau, D.; Dai, M.; Estéve, A.; Chabal, Y. J. *Nat. Mater.* **2010**, *9*, 266−271.
(9) Wang, X.; Ruther, R. E.; Streifer, J. A.; Hamers, R. J. *J. Am. Chem. Soc.* **2010**, *132*, 4048−4049.
(10) Rijksen, B.; van Lagen, B.; Zuilhof, H. *J. Am. Chem. Soc.* **2011**, *133*, 4998−5008.
(11) Higashi, G. S.; Chabal, Y. J.; Trucks, G. W.; Raghavachari, K. *Appl. Phys. Lett.* **1990**, *56*, 656−658.
(12) Clark, I. T.; Aldinger, B. S.; Gupta, A.; Hines, M. A. *J. Phys. Chem. C* **2010**, *114*, 423−428.
(13) Hines, M. A.; Chabal, Y. J.; Harris, T. D.; Harris, A. L. *J. Chem. Phys.* **1994**, *101*, 8055−8072.
(14) Allongue, P.; Kieling, V.; Gerischer, H. *Electrochim. Acta* **1995**, *40*, 13553−11360.
(15) Hines, M. A.; Faggin, M. F.; Gupta, A.; Aldinger, B. S.; Bao, K. *J. Phys. Chem. C* **2012**, *116*, 18920−18929.
(16) Wade, C. P.; Chidsey, C. E. D. *Appl. Phys. Lett.* **1997**, *71*, 1879−1881.
(17) Judge, J. S. *J. Electrochem. Soc.* **1971**, *118*, 1772−1775.
(18) Trucks, G. W.; Raghavachari, K.; Higashi, G. S.; Chabal, Y. J. *Phys. Rev. Lett.* **1990**, *65*, 504−507.
(19) Trucks, G. W.; Raghavachari, K.; Higashi, G. S.; Chabal, Y. J. *Phys. Rev. Lett.* **1991**, *66*, 1648.
(20) Aldinger, B. S.; Clark, I. T.; Gupta, A.; Hines, M. A. *J. Appl. Phys.* **2010**, *107*, 103520.
(21) Clark, I. T.; Aldinger, B. S.; Gupta, A.; Hines, M. A. *J. Chem. Phys.* **2008**, *128*, 144711.
(22) Faggin, M. F.; Hines, M. A. *Rev. Sci. Instrum.* **2004**, *75*, 4547−4553.
(23) *Mathematica*, version 8.0; Wolfram Research, Inc.: Champaign, IL, 2011.
(24) Kolasinski, K. W. *J. Electrochem. Soc.* **2005**, *152*, J99−J104.
(25) *CRC Handbook of Chemistry and Physics*, 92nd ed.; Haynes, W. M., Ed.; Chapman & Hall/CRC Press: Boca Raton, FL, 2012.
(26) Northrup, J. E. *Phys. Rev. B* **1991**, *44*, 1419−1422.
(27) Freking, U.; Krüger, P.; Mazur, A.; Pollmann, J. *Phys. Rev. B* **2004**, *69*, 035315.
(28) Jakob, P.; Chabal, Y. J.; Kuhnke, K.; Christman, S. B. *Surf. Sci.* **1994**, *302*, 49−56.
(29) Watanabe, S. *Surf. Sci.* **1996**, *351*, 149−155.
(30) Jakob, P.; Chabal, Y. J. *J. Chem. Phys.* **1991**, *95*, 2897−2909.
(31) Faggin, M. F.; Green, S. K.; Clark, I. T.; Queeney, K. T.; Hines, M. A. *J. Am. Chem. Soc.* **2006**, *128*, 11455−11462.
(32) Jakob, P.; Chabal, Y. J.; Raghavachari, K. *Chem. Phys. Lett.* **1991**, *187*, 325−333.
(33) Newton, T. A.; Boiani, J. A.; Hines, M. A. *Surf. Sci.* **1999**, *430*, 67−79.
(34) Dumas, P.; Chabal, Y. J.; Jakob, P. *Surf. Sci.* **1992**, *269/270*, 867−878.
(35) Bjorkman, C. H.; Fukuda, M.; Yamazaki, T.; Miyazaki, S.; Hirose, M. *Jpn. J. Appl. Phys.* **1995**, *34*, 722−726.
(36) Kanaya, H.; Usuda, K.; Yamada, K. *Appl. Phys. Lett.* **1995**, *67*, 682−684.
(37) Wade, C. P.; Chidsey, C. E. D. *Appl. Phys. Lett.* **1997**, *71*, 1879−1881.
(38) Garcia, S. P.; Bao, H.; Manimaran, M.; Hines, M. A. *J. Phys. Chem. B* **2002**, *106*, 8258−8264.
(39) Bassindale, A. R.; Taylor, P. G. In *The chemistry of organic silicon compounds*. Patai, S., Rappaport, Z., Eds.; Wiley: New York, NY, 1989, 809−838.

(40) Dijkstra, T. W.; Duchateau, R.; van Santen, R. A.; Meetsma, A.; Yap, G. P. A. *J. Am. Chem. Soc.* **2002**, *124*, 9856−9864.
(41) Leung, K.; Nielsen, I. M.; Criscenti, L. J. *J. Am. Chem. Soc.* **2009**, *131*, 18358−18365.
(42) Sacher, E.; Yelon, A. *Phys. Rev. Lett.* **1991**, *66*, 1647.
(43) Steward, O. W.; Pierce, O. R. *J. Am. Chem. Soc.* **1961**, *83*, 4932−4936.
(44) Cartledge, F. K. *Organometallics* **1983**, *2*, 425−430.
(45) Jehng, W.-D.; Lin, J.-C.; Lee, S.-L. *J. Electrochem. Soc.* **2005**, *152*, C124−C130.
(46) Chabal, Y. J. *Surf. Sci. Rep.* **1988**, *8*, 211−357.